Kovove Mater. 64 2026 251–261
DOI: 10.31577/km.2026.5.251

Tribological characterization of magnesium matrix nanocomposites prepared by spark plasma sintering

Viktor Puchý[1]*, Róbert Džunda[1], Mária Podobová[1], Lucia Čiripová[1], Ondrej Petruš[1], Michal Besterci[1]

[1]*Institute of Materials Research, SAS, Watsonova 47, 040 01 Košice, Slovak Republic*

Received 2 August 2026, received in revised form 2 October 2026, accepted 7 October 2026

Abstract

This study investigated the effect of short SiC nanofiber content on the microstructure, microhardness, friction behavior, tribofilm stability, and wear mechanisms of magnesium composites prepared by spark plasma sintering. Unreinforced Mg (H1) was compared with Mg-3 wt.% SiC_{nf}-1 wt.% GNP (H3) and Mg-6 wt.% SiC_{nf}-1 wt.% GNP (H6) composites. Prior to tribological testing, a temporary graphite layer was mechanically applied to the polished surfaces. Reciprocating sliding tests against a 6 mm diameter ZrO_2 ball were performed under normal loads of 3 and 5 N at a frequency of 1 Hz, a stroke length of 5 mm, and a total of 1000 complete cycles. The microstructure, wear-track morphology, and elemental distribution were examined by optical microscopy, SEM/EDS, and 3D profilometry. The composites exhibited a network-like distribution of reinforcing constituents, predominantly along the interfaces of Mg-rich regions. The highest microhardness, 65.6 ± 4.7 HV0.1, was measured for H3. At 3 N, H3 and H6 maintained a stable coefficient of friction of approximately 0.15–0.17 throughout the entire test, whereas H1 exhibited an increase above 0.30 after approximately 450 s. At 5 N, failure of the low-friction regime occurred after approximately 270 s for H1, 680 s for H3, and 920 s for H6. The lowest wear rates were recorded for H6, reaching 4.9×10^{-6} mm^3 N^{-1} m^{-1} at 3 N and 1.72×10^{-4} mm^3 N^{-1} m^{-1} at 5 N. The improved tribological performance of the composites was associated with the mechanical support of a heterogeneous carbon-oxide tribofilm by the SiC nanofibers. H3 exhibited the most favorable friction behavior at 3 N, whereas H6 provided the highest load-bearing capacity and the lowest wear rate under both applied loads.

K e y w o r d s: magnesium matrix composites, SiC nanofibers, graphene nanoplatelets, spark plasma sintering, coefficient of friction

1. Introduction

Magnesium and its alloys are among the lightest metallic structural materials and, owing to their low density, high specific strength, and good machinability, are promising candidates for the transportation, aerospace, electronics, and other industries in which component weight reduction is of primary importance. However, their wider use in tribologically loaded components is limited by their relatively low hardness, poor resistance to surface plastic deformation, and high susceptibility to abrasive, adhesive, and delamination wear. Under dry sliding conditions, repeated shear loading of the Mg matrix may lead to microploughing, material smearing, subsurface crack formation, and the subsequent detachment of surface lamellae. Tribo-oxidation of freshly exposed magnesium also plays an important role because the resulting oxide products may contribute to the formation of a protective mechanically mixed layer; however, after fragmentation, they may also act as abrasive third-body particles [1–6]. One approach to improving the tribological properties of Mg-based materials is the incorporation of a hard ceramic reinforcement. Silicon carbide is characterized by high hardness, stiffness, and thermal stability and, when introduced into

*Corresponding author: e-mail address: vpuchy@saske.sk

This article is distributed under the terms of the Creative Commons Attri-bution-NonCommercial 4.0 International Public License (CC BY-NC 4.0).

an Mg matrix, may increase resistance to counterbody penetration, restrict plastic flow, and carry part of the contact load. Experimental studies involving SiC nanoparticles have demonstrated increased hardness, microstructural refinement, and improved sliding wear resistance of Mg and AZ31 or AZ80 alloys [7, 13–15]. However, the effect of SiC is not universally beneficial. Insufficient dispersion, excessive reinforcement content, or inadequate bonding at the matrix-reinforcement interface may promote the formation of agglomerates, residual porosity, and local stress concentrators. Detached or fragmented SiC particles may subsequently enter the sliding contact and promote three-body abrasion. The resulting tribological behavior therefore depends not only on the nominal reinforcement content but also on its morphology, distribution, and interfacial bonding with the Mg matrix.

An alternative approach is the use of carbon nanomaterials with low shear strength, particularly graphene nanoplatelets. GNPs may perform a dual function: they can mechanically reinforce the matrix and, after being exposed or released from the surface, contribute to the formation of a carbon-rich tribological layer. Several studies on Mg-GNP composites have reported a decrease in the coefficient of friction, reduced mass or volume loss, and smoother wear tracks with less extensive delamination [1–6]. Arab and Marashi observed a reduction in the coefficient of friction of approximately 25–45 % for GNP-reinforced AZ31 compared with the unreinforced material and attributed the improvement to the combined effects of increased hardness and the formation of a lubricating layer [1]. Similarly, Wu et al. and Lu et al. observed reduced friction and wear in AZ31 composites as a result of a protective carbonaceous film and reduced direct contact between the counterbody and the Mg matrix [2, 3]. The effect of GNPs, however, strongly depends on their content and distribution. A low to moderate content may promote load transfer, microstructural refinement or stabilization, and the formation of a low-shear layer. At excessive volume fractions, however, the tendency toward agglomeration, pore formation, and reduced local cohesion of the composite increases. Lu et al., for example, observed increasing porosity with increasing GNP content in AZ31 composites [3]. Kandemir et al. confirmed that the presence of GNPs in ZE10/GNP composites may improve friction stability and reduce wear, while also affecting porosity and mechanical properties depending on reinforcement concentration and processing conditions [6]. The mere presence of carbon on a worn surface therefore does not necessarily indicate the formation of an effective tribofilm. Its coverage of the real contact areas, cohesion, ability to regenerate, and mechanical support by the substrate are decisive. Combining a hard ceramic reinforcement with a carbon-based lubricating constituent represents the concept of a hybrid self-lubricating composite. SiC may provide load-bearing capacity and resistance to penetration within the near-surface region, whereas graphite, graphene, or reduced graphene oxide may reduce shear stress at the interface between the sliding bodies. For Mg-SiC--graphite hybrid composites, Prakash et al. demonstrated that the addition of graphite to an Mg-SiC system may reduce wear and the coefficient of friction through the formation of a mechanically mixed layer, although higher contents of the carbonaceous constituent may increase delamination and brittle surface failure [8]. Al-Maamari et al. observed the formation of a graphite-rich layer on tribologically loaded surfaces of Mg-SiC-graphite composites and emphasized the importance of balancing hardness, SiC content, and the lubricating effect of graphite [9]. A similar synergistic effect was investigated by Kavimani et al. in Mg composites reinforced with SiC-modified reduced graphene oxide [10, 11]. Increasing the SiC content initially improved wear resistance; however, once the optimum concentration was exceeded, wear increased again. Abrasive and delamination wear mechanisms were identified on the worn surfaces, and their severity depended on reinforcement content, applied load, and the stability of the resulting tribolayer. These findings indicate that an optimum hybrid composite cannot be designed simply by maximizing the content of the hard reinforcement. Although an excessive SiC content may increase the hardness and nominal load-bearing capacity of the matrix, it may also promote interfacial defects and the generation of hard third-body particles. Most published studies have focused on composites in which the graphite or graphene constituent is incorporated directly into the metallic matrix. Less attention has been paid to Mg composites in which an internal carbon reinforcement is combined with a temporary, mechanically applied graphite layer on the initial surface. Such a layer may act as a reservoir of low-shear material during running-in. During repeated sliding, the graphite is spread, compacted, and mixed with oxides and metallic wear products, potentially forming a dynamic carbon-oxide mechanically mixed layer. Its functional lifetime, however, depends on the ability of the underlying material to resist plastic deformation, subsurface cracking, and delamination. On soft, unreinforced Mg, the graphite layer may be rapidly displaced from the real contact areas, whereas a SiC-reinforced matrix may provide greater mechanical support. At excessively high SiC contents, however, the continuity of the film may be disrupted by released hard fragments [8–12]. The tribological effect of the hybrid reinforcement also depends on the applied normal load. Increasing the load enlarges the real contact area, enhances counterbody penetration, and increases subsurface shear stress, thereby potentially accelerating failure of the tribological layer. Conversely, a higher contact pressure may promote

the compaction of graphite and oxide particles into a denser mechanically mixed layer. The resulting response is therefore governed by competition between tribofilm formation and compaction on the one hand, and its removal, delamination, and the generation of abrasive particles on the other. Previous results for Mg-GNP, Mg-SiC, and hybrid Mg-SiC-carbon composites have confirmed that the dominant mechanism may vary with applied load, sliding distance, and reinforcement concentration [1, 6, 8–13].

The aim of the present study was therefore to clarify the effect of short SiC nanofiber content on friction, the stability of a graphite-carbon tribofilm, and the wear mechanisms of Mg composites containing 1 wt.% GNPs. Unreinforced Mg, designated H1, was compared with H3 and H6 composites containing 3 and 6 wt.% SiC_{nf}, respectively. Before the reciprocating tribological tests, a temporary graphite-rich layer was mechanically applied to the polished surfaces using a graphite pencil. The tests were conducted against a 6 mm diameter ZrO_2 ball under normal loads of 3 and 5 N, at a frequency of 1 Hz and a stroke length of 5 mm. The time-dependent evolution of the coefficient of friction was correlated with the microstructure of the starting materials and with the morphology and chemical composition of the wear tracks examined by optical microscopy and SEM/EDS. Particular attention was paid to the transition from a stable low-friction regime to a high-friction regime following tribofilm failure, and to the different roles of 3 and 6 wt.% SiC_{nf} under moderate and higher contact loads.

2. Materials and methods

Magnesium powder (∼ 325 mesh powder with purity 99.5 %, Thermo Scientific Chemicals) with the addition of 3 and 6 wt.% of silicon carbide milled nanofibers (Sigma-Aldrich) have been used as the base materials. The above powders were mixed with the addition of 1 wt.% of GNPs (graphene nanoplatelets aggregates with a specific surface area 500 $m^2\,g^{-1}$, sub-micron particles powder, Alfa Aesar). The mixing process was performed using a three-dimensional mixing device "Turbula". All powders were milled with a rotation velocity of 33 rpm for 3 h. Finally, the mixtures were sintered using SPS (HP D 10SD, FCT Systeme, Frankenblick, Germany) in the temperatures 500 ℃ for 5 min. with uniaxial pressure of 64 MPa (20 kN). The sintered compacts were disc-shaped, measuring 20 mm in diameter and approximately 4 mm in height. The sample surfaces were then ground and mechanically polished. The hardness was determined by the Vickers method. After sintering the local microstructures were analyzed using a Light Microscope Olympus GX 71. Prior to tribological testing,

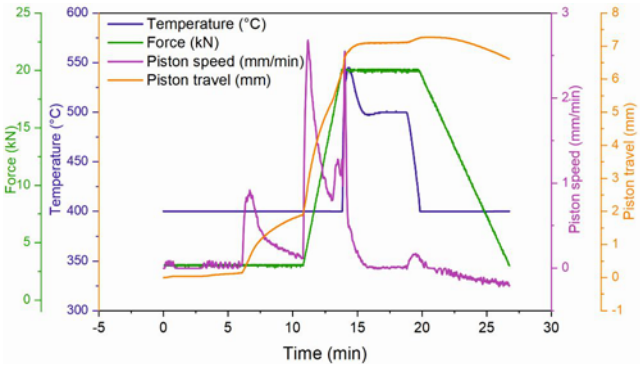


Fig. 1. SPS profiles for the Mg-3 wt.% SiC_{nf}-1 wt.% GNP composite. Temperature, axial force, piston travel and piston velocity versus time.

a graphite-rich surface layer was mechanically applied to all polished specimens. Graphite was removed from the wooden Graphite-rich pencil and finely ground in an agate mortar until a homogeneous powder was obtained. A fixed amount of the resulting powder was uniformly distributed on a clean metallographic polishing cloth, and the polished specimen surfaces were subsequently burnished using the same metallographic polishing procedure for all materials. The polishing time was 5 min. and amount of graphite-rich powder were kept constant for each specimen. After burnishing, loosely attached particles were removed by a gentle air stream, leaving only the mechanically adhered graphite-rich surface layer. Tribological tests were conducted on an automatic tribometer (Bruker UMT2) under reciprocal dry sliding conditions, employing a ball-on-flat configuration at room temperature and atmospheric pressure. A 6 mm diameter ZrO_2 ceramic ball was used as the friction counterpart. All tests were performed with a 3 and 5 N normal load, a sliding velocity of 0.01 $m\,s^{-1}$, and a track length of 5 mm, covering a total sliding distance of 10 m. After tribological tests, the worn surfaces were analyzed by SEM equipped with EDS (Tescan Vega-3 LMU, Brno, Czech Republic; Bruker XFlash Detector 410-M, Billerica, MA, USA). The morphology of wear tracks and the wear mechanisms were evaluated by a confocal 3D optical profiler (PLu neox, SENSOFAR, Barcelona, Spain). The wear rate was calculated from the mean cross-sectional area of three profiles measured at different positions across each wear track. The reported values are expressed as mean ± sample standard deviation ($n = 3$).

3. Results and discussion

3.1. Sintering parameters

The composites were consolidated by spark plasma sintering under vacuum using the same sintering

schedule for all samples. Figure 1 shows the SPS sintering cycle for the representative Mg-3 wt.% SiC nanofiber composite. Following the initial evacuation and stabilization stage, the sample was maintained under a preliminary force of 3 kN for approximately 350 s. This was followed by low-power preheating while the applied force remained constant. From approximately 650 s onward, the pressing force was gradually increased from 3 to 20 kN while the sample was simultaneously heated to the target temperature of 500 ℃. The maximum force of 20 kN was reached after approximately 820 s and was subsequently maintained throughout the isothermal holding stage. The target temperature of 500 ℃ was maintained for approximately 5 min. During the transition to pyrometric temperature control, a short-term temperature overshoot to approximately 545 ℃ was recorded, after which the temperature stabilized at 500 ℃. Following completion of the holding stage, the sample was cooled to approximately 400 ℃ while the maximum pressing force was maintained. The force was then gradually reduced to 3 kN during further cooling. The total recorded cycle time was approximately 1600 s, corresponding to approximately 27 min. Pyrometric temperature measurement commenced at approximately 400 ℃; therefore, lower temperatures during the preheating stage were not recorded. During heating and loading, the relative punch displacement of the representative H3 composite gradually increased to approximately 7 mm. The most pronounced displacement occurred during the increase in pressing force and upon approaching the sintering temperature. This behavior indicates intensive densification of the powder mixture before the isothermal holding stage, followed by stabilization of the dimensional changes during sintering.

3.2. Microstructures

Optical microscopy revealed the characteristic morphology and phase distribution of the sintered materials in Fig. 2. The microstructure of sample H1, shown in Fig. 2a, consists of polyhedral grains of the metallic matrix with clearly defined grain boundaries. Local defects and pores are visible within the structure, which are common features of powder metallurgy processing. The matrix is relatively homogeneous and contains no secondary reinforcing phases. The micrograph of sample H3 (Fig. 2b) shows a typical network structure. The reinforcing constituents, visible as black and dark-grey regions, are not homogeneously distributed within the grain interiors but are preferentially segregated along the boundaries of the primary magnesium grains. This spatial distribution results from the processing route, during which the SiC nanofibers and graphene nanoplatelets mechanically coat the surfaces of the initial magnesium powder particles and, after consolidation, form a semi-continuous network surrounding the individual metallic grains.

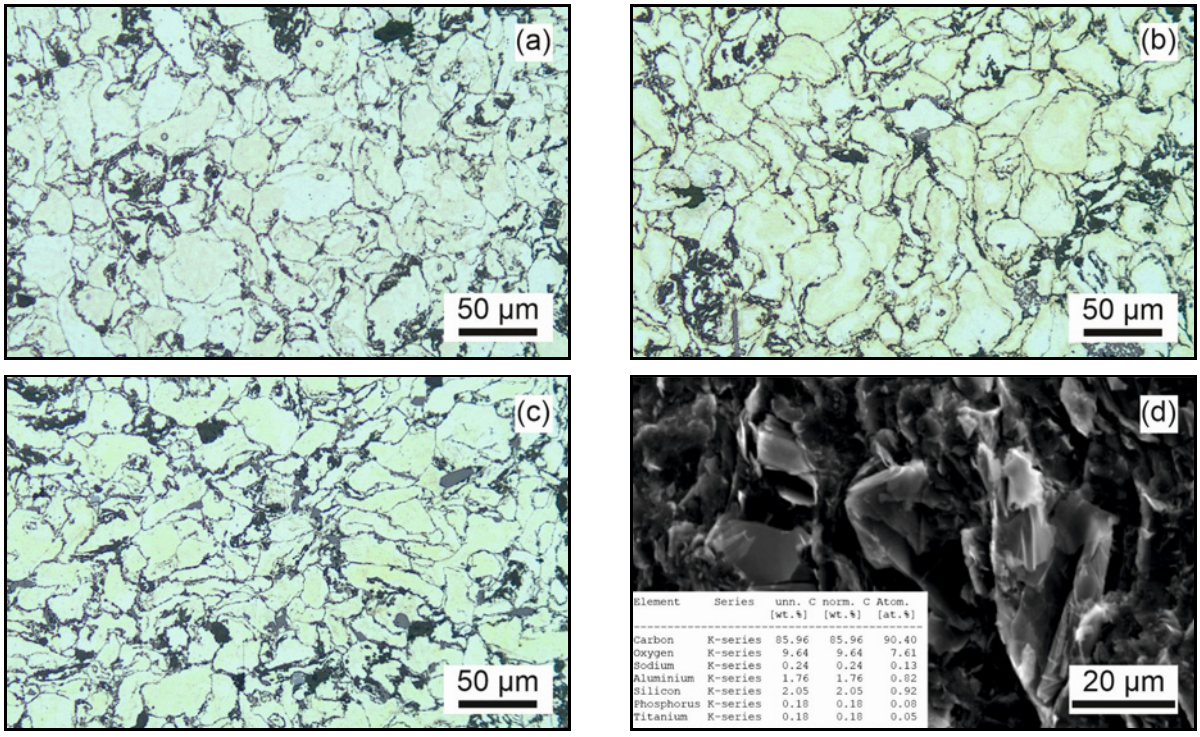


Fig. 2. Microstructure of reference Mg material (a), Mg-3 wt.% SiC_{nf}-1 wt.% GNP composite (b), Mg-6 wt.% SiC_{nf}-1 wt.% GNP composite (c), and graphite pencil (d).

The morphology of the H6 composite shown in Fig. 2c confirms the preservation of the same network structure as in H3. Owing to the higher volume fraction of SiC nanofibers, however, the reinforcement network along the grain boundaries is thicker and more continuous. The increased content of secondary constituents results in a more pronounced separation of the magnesium matrix grains and a greater occurrence of larger reinforcement agglomerates, which are concentrated mainly at triple-junction regions. This specific architecture, characterized by the segregation of the hard SiC_{nf} phase and the lubricating GNP phase along the grain boundaries, directly influences the tribological behavior of the materials. During surface wear, the continuous network of ceramic nanofibers acts as a load-bearing skeleton that resists plastic deformation, whereas the solid lubricant in the form of GNPs is released from these interfacial regions into the contact zone, thereby promoting the formation and replenishment of a protective tribofilm.

3.3. Mechanical properties

The microhardness of the investigated materials was determined using the Vickers method at a load of HV0.1 and a dwell time of 15 s. The unreinforced Mg material, designated H1, exhibited an average hardness of 61.8 ± 3.4 HV0.1. The addition of 3 wt.% SiC nanofibers and 1 wt.% GNPs increased the hardness of the H3 composite to 65.6 ± 4.7 HV0.1, corresponding to an increase of approximately 6 % compared with pure Mg. This increase may be attributed to the restriction of local plastic deformation of the Mg matrix, load transfer to the SiC nanofibers, and increased resistance to dislocation motion at the matrix-reinforcement interfaces. When the SiC_{nf} content was increased to 6 wt.%, the H6 composite reached a hardness of 62.9 ± 3.9 HV0.1. This value was only approximately 2 % higher than that of pure Mg and approximately 4 % lower than that of H3. The result indicates that increasing the reinforcement content above 3 wt.% did not lead to a further increase in local microhardness. A likely explanation is the greater microstructural heterogeneity of H6, including local nanofiber agglomeration, porosity, or insufficiently cohesive interfaces, which may partly offset the strengthening effect of the higher SiC_{nf} content. The average hardness values followed the order H3 > H6 > H1. However, the differences between the mean values were relatively small compared with the corresponding standard deviations, and the ranges of the individual measurements overlapped. The results should therefore be interpreted primarily as a trend rather than as unambiguous evidence of statistically significant differences among the materials. It was also shown that the lowest wear rate of H6 was not directly proportional to its average microhardness. In addition to hardness, the tribological resistance was influenced by the distribution of the reinforcement, the load-bearing capacity of the subsurface region, and the stability of the carbon-oxide tribofilm.

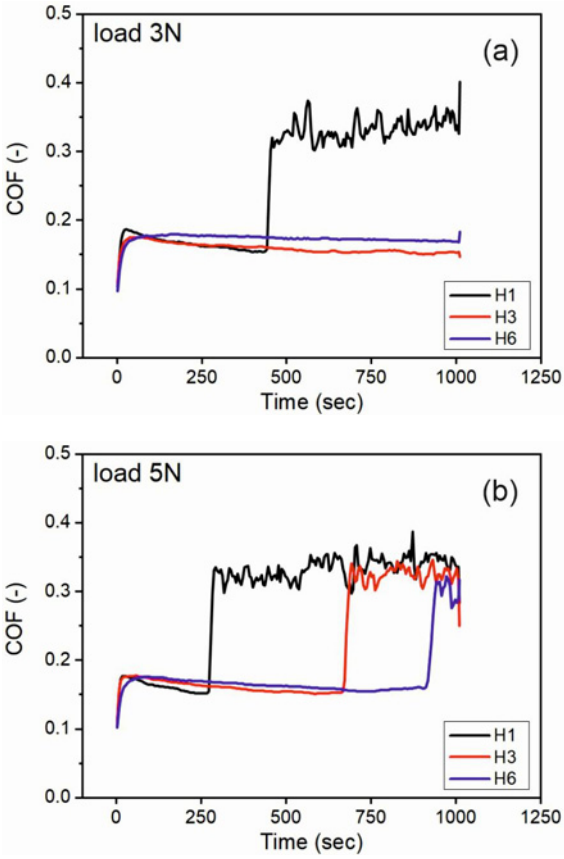


Fig. 3. Coefficient of friction (COF) of materials at 3 N (a) and 5 N (b).

3.4. Coefficient of friction

Before the tribological tests was mechanically burnished graphite-rich layer to the polished surfaces of the samples. This layer did not constitute a firmly bonded coating, but rather a temporary reservoir of carbonaceous material that was progressively spread, fragmented, compacted, and mixed with wear debris during reciprocating sliding. Consequently, a dynamic mechanically mixed layer was likely formed within the contact zone, consisting of graphite from the pencil, Mg-containing debris, magnesium oxides, and, in the case of the composites, also GNPs and particles originating from the SiC nanofibers. The evolution of the coefficient of friction (COF) shown in Fig. 3 during reciprocating sliding against a ZrO_2 ball exhibited a pronounced dependence on the presence of the reinforcing phases, SiC_{nf} and GNPs, as well as on the applied normal load. It is generally recognized that the incorporation of nanoparticles and carbon-based structures can

markedly improve the tribological behavior of magnesium alloys by reducing adhesive wear [16]. At a load of 3 N (Fig. 3a), the reference material H1, consisting of pure Mg, initially exhibited a stable COF of approximately 0.17–0.18. However, after about 450 s of testing, an abrupt transition occurred, accompanied by an increase in COF above 0.30 and a maximum value of 0.37. In contrast, the H3 and H6 composites maintained a stable COF in the range of 0.15–0.17 throughout all 1000 cycles, with no indication of lubricating-film failure. These findings are consistent with literature data showing that graphene- and graphite-containing phases can reduce the COF owing to their lubricating properties and their ability to limit brittle failure of near-surface layers [17, 18]. Increasing the normal load to 5 N (Fig. 3b) led to a transition toward a boundary-friction regime in all samples. Sample H1 failed after approximately 270 s, after which pronounced COF fluctuations were observed, with a maximum value of 0.39 reached at approximately 870 s. The presence of reinforcement in the composite materials progressively delayed tribofilm breakdown. Sample H3, containing 3 wt.% SiC_{nf}, maintained a stable COF below 0.17 up to approximately 680 s, followed by an abrupt increase above 0.34. The H6 composite, containing 6 wt.% SiC_{nf}, exhibited the highest load-bearing capacity, with tribofilm stability and a COF of approximately 0.16–0.17 maintained until about 920 s. The higher content of the hard ceramic SiC phase therefore improved the load-bearing capacity of the contact zone under increased normal loading [19].

3.5. Wear mechanisms

SEM observations and EDS elemental mapping in Fig. 4 supported the measured tribological data. In pure magnesium (H1) in Fig. 4a, severe abrasive and adhesive wear dominated under both applied loads. The worn surfaces were characterized by deep ploughing grooves and extensive plastic deformation. This behavior primarily resulted from degradation of the soft, unreinforced magnesium matrix under contact with the harder counterbody. The EDS maps of the H1 wear tracks indicated extensive oxidation and a locally absent carbon signal within the wear scar, suggesting rapid destruction and displacement of the temporary graphite layer from the contact zone. The H3 and H6 composites tested at 3 N exhibited markedly different surface morphologies, characterized by relatively smooth wear tracks with limited evidence of abrasion. EDS elemental mapping revealed the presence of a continuous carbon-rich film within the contact zone, which was preserved owing to the mechanical stabilization provided by the SiC_{nf} reinforcement. At a load of 5 N, the composites also underwent a gradual transition toward a severe-wear regime. Deeper grooves and local surface delamination were observed, consistent with tribofilm failure toward the end of the test. Similar increases in local delamination and oxidation of Mg matrices after exceeding critical contact loads have been reported in studies investigating the effect of contact pressure [20]. EDS mapping of the worn surfaces confirmed the presence of carbon and oxygen within all wear tracks. The distribution of carbon suggests that the graphite mechanically applied before testing was not completely removed from the contact but was redistributed during reciprocating sliding and incorporated into a mechanically mixed surface layer. In the H3 in Fig. 4b and H6 composites in Fig. 4c, the carbonaceous component of the tribofilm may additionally have been replenished by GNPs released from the Mg matrix. The simultaneous presence of oxygen indicates tribo-oxidation of Mg and the formation of a mixed carbon-oxide film containing graphite particles, Mg oxide products, and fine metallic debris [6]. On the unreinforced H1 surface, this layer was insufficiently supported mechanically. Extensive grooving, plastic smearing, and lamellar delamination indicate that the soft Mg matrix underwent intensive plastic deformation. The graphite film was locally displaced or disrupted, resulting in repeated exposure and oxidation of fresh Mg surfaces. Wear of H1 was therefore governed by a combination of microploughing, adhesive smearing, tribo-oxidation, and fatigue delamination. The addition of 3 wt.% SiC_{nf} and 1 wt.% GNPs in H3 markedly improved surface stability. The SiC nanofibers increased the local load-bearing capacity of the matrix and restricted penetration of the ZrO_2 counterbody, whereas the GNPs, together with the initially applied graphite, promoted the formation of a low-shear carbonaceous layer. Such synergistic action between hard SiC reinforcement and a lubricating graphite component has also been observed in hybrid Mg-SiC-graphite composites [9]. The relatively uniform distributions of C and O and the limited extent of delamination are consistent with the formation of a more cohesive mechanically mixed layer. Consequently, H3 predominantly exhibited mild abrasive wear accompanied by local adhesive smearing. When the SiCnf content was increased to 6 wt.%, plastic deformation of the Mg matrix remained restricted, although the H6 surface became more heterogeneous. The greater number of Si-rich regions and local defects suggests exposure or release of SiC-containing particles. These particles may have entered the contact as hard third-body debris, promoting local microcutting and disrupting the continuity of the carbon-oxide tribofilm. The higher SiC_{nf} content therefore improved the load-bearing capacity of the matrix but simultaneously increased the probability of three-body abrasion [9]. In terms of tribofilm stability and the overall extent of surface damage, H3 represented a more favorable configuration than H6 at 3 N.

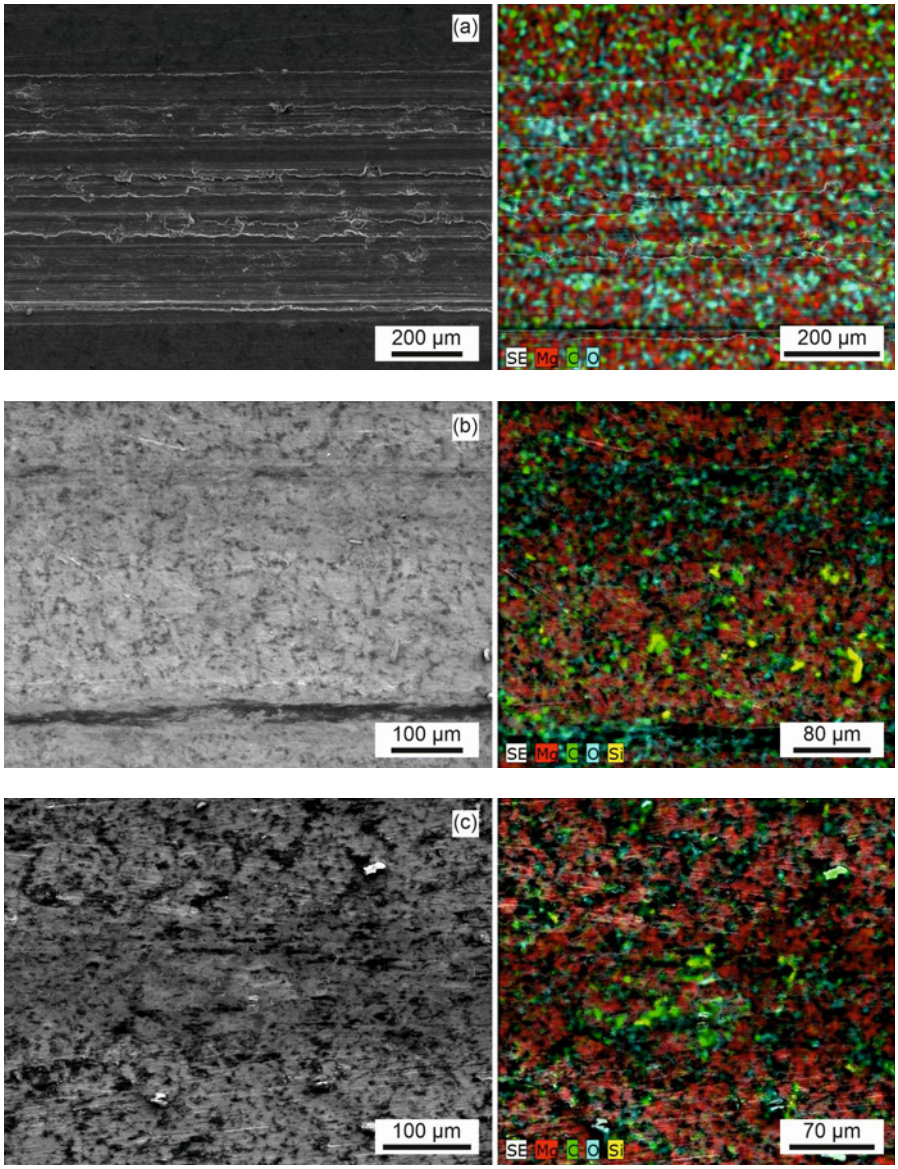


Fig. 4. SEM and EDS maps of wear tracks on pure Mg (a), Mg-3 wt.% SiC_{nf}-1 wt.% GNP composite (b), and Mg-6 wt.% SiC_{nf}-1 wt.% GNP composite (c) after translational slip testing against a ZrO_2 ceramic ball.

EDS mapping of the wear tracks formed at a load of 5 N confirmed the presence of carbon and oxygen on the surfaces of all investigated materials. Carbon originated primarily from the graphite layer mechanically applied before testing, whereas in the H3 and H6 composites the tribofilm may also have been continuously replenished by GNPs released from the Mg matrix. The presence of oxygen indicates tribo-oxidation of freshly exposed magnesium. During reciprocating sliding, carbonaceous, oxide, and metallic wear products were repeatedly spread and compacted, resulting in the formation of a heterogeneous carbon-oxide mechanically mixed layer [6]. On the unreinforced H1 surface, this layer was insufficiently supported mechanically. The soft Mg matrix underwent intensive microploughing, plastic flow, and adhesive smearing. The graphite film was displaced from highly loaded regions, pressed into grooves, and fragmented together with Mg-oxide products. Repeated exposure and oxidation of fresh Mg promoted the formation of harder third-body particles and further abrasive damage. Wear of H1 in Fig. 4a was therefore governed by a combination of plastic deformation, abrasion, tribo-oxidation, and fatigue delamination. The addition of 3 wt.% SiC_{nf} and 1 wt.% GNPs in H3 increased the local load-bearing capacity of the Mg matrix and promoted the formation of a carbon-oxide tribofilm in Fig. 4b. At a load of 5 N, however, the SEM morphology revealed extensive lamellar delamination and the accumulation of plastically deformed wear products. The mechanically mixed layer was repeatedly formed and compacted, but high shear stresses caused it to crack and

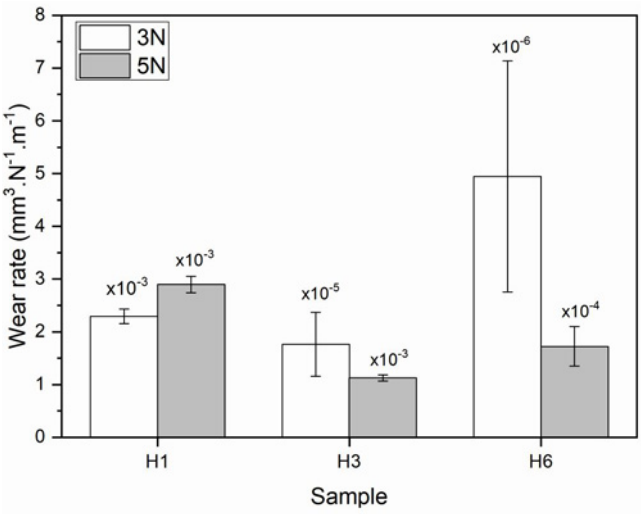


Fig. 5. Wear rate graph of Mg, Mg-3 wt.% SiC_{nf}-1 wt.% GNP composite and Mg-6 wt.% SiC_{nf}-1 wt.% GNP composite at velocity of 0.01 m s^{-1}, length of 10 m and normal load of 3 and 5 N.

detach together with the subsurface-deformed material. Local Si-rich regions suggest that released SiC--containing fragments may have contributed to three--body abrasion. When the SiC_{nf} content was increased to 6 wt.%, large-scale plastic deformation of the Mg matrix was suppressed more effectively. The reinforced substrate provided better mechanical support for the carbon-oxide tribofilm and restricted penetration of the ZrO_2 counterbody. However, the EDS map of H6 in Fig. 4c revealed numerous local Si-rich regions, which may be associated with exposure, fragmentation, or pull-out of the SiC reinforcement. These hard fragments may have locally disrupted the continuity of the tribofilm and promoted microcutting. Despite this mechanism, the damage in H6 remained more spatially localized than in H1 and H3. The results demonstrate that the effect of SiCnf content was load-dependent. At 3 N, H3 provided the most favorable balance between matrix strengthening and carbon tribofilm stability, whereas at 5 N the higher load-bearing capacity of H6 became the dominant factor. The increased SiC_{nf} content restricted large-scale plastic flow and delamination, although it simultaneously increased the risk of local three-body abrasion caused by released SiC-containing particles [9].

3.6. Wear rate

The wear rate was calculated from the mean cross-sectional area of three wear-track profiles (Fig. 5). For a stroke length of 5 mm and 1000 complete reciprocating cycles, the total sliding distance was 10 m. The wear volume was approximated as the product of the mean cross-sectional area and the wear-track length. The reported deviations represent the sample standard deviation of three profiles measured at different positions along the same wear track. At a load of 3 N, the unreinforced H1 material exhibited a wear rate of $(2.29 \pm 0.14) \times 10^{-3}$ mm^3 N^{-1} m^{-1}. The H3 composite containing 3 wt.% SiC_{nf} and 1 wt.% GNPs showed a value of $(1.76 \pm 0.61) \times 10^{-5}$ mm^3 N^{-1} m^{-1}, whereas the lowest value, $(4.9 \pm 2.2) \times 10^{-6}$ mm^3 N^{-1} m^{-1}, was measured for H6 containing 6 wt.% SiC_{nf} and 1 wt.% GNPs. Compared with unreinforced Mg, the wear rate decreased by more than 99 % for both H3 and H6. These results demonstrate that the incorporation of SiC nanofibers markedly improved the resistance of the Mg matrix to volumetric material loss. An improvement in the wear resistance of Mg composites following the addition of SiC or GNPs was also reported by Das and Harimkar [7], who highlighted the existence of an optimum reinforcement content, above which agglomeration and microstructural defects may cause the wear rate to increase again. Although H3 exhibited the lowest and most stable coefficient of friction at 3 N, the smallest geometrical material loss was recorded for H6. Thus, friction reduction and wear reduction were not governed by entirely identical mechanisms. In H3, the low shear strength and stability of the carbon-oxide tribofilm played the predominant role, whereas in H6 the higher load-bearing capacity of the composite matrix and the more effective restriction of counterbody penetration became more pronounced. The higher coefficients of variation observed for H3 and H6 indicate local heterogeneity of the very shallow wear tracks, which may be associated with non-uniform tribofilm compaction, the local presence of SiC-containing particles, and variations in the degree of plastic deformation. At a load of 5 N, H1 exhibited a wear rate of $(2.90 \pm 0.16) \times 10^{-3}$ mm^3 N^{-1} m^{-1}. The addition of 3 wt.% SiC_{nf} and 1 wt.% GNPs reduced the value for H3 to $(1.13 \pm 0.06) \times 10^{-3}$ mm^3 N^{-1} m^{-1}, while the lowest value of $(1.72 \pm 0.38) \times 10^{-4}$ mm^3 N^{-1} m^{-1} was obtained for H6. Compared with unreinforced Mg, this corresponds to reductions of approximately 61 % for H3 and 94 % for H6. The wear rate of H6 was approximately 85% lower than that of H3, demonstrating the beneficial effect of the higher SiC_{nf} content on the load-bearing capacity of the composite under the higher contact load. This result is consistent with the longest lifetime of the low-friction regime observed for H6 at 5 N. Despite the local formation of SiC--containing third-body debris, the beneficial effect of the increased load-bearing capacity of the matrix remained dominant. The higher SiC nanofiber content most effectively increased the load-bearing capacity of the matrix and restricted penetration of the ZrO_2 ball. The higher coefficient of variation of H6, approximately 22 %, indicates local heterogeneity of the shallower wear track. This may be related to non-uniform

preservation of the tribofilm, local SiC_{nf} agglomerates, reinforcement pull-out, or variations in the intensity of three-body abrasion. Despite its greater relative variability, the absolute wear rate of H6 remained clearly the lowest. For H1, increasing the load caused only a relatively moderate increase in the wear rate because the surface had already entered a severe plastic-deformation and delamination-wear regime at 3 N. In contrast, the H3 and H6 composites exhibited exceptionally shallow wear tracks at 3 N; consequently, increasing the load to 5 N resulted in an increase of several orders of magnitude in their wear rates. Nevertheless, H6 retained a substantial advantage over H1 and H3 even at 5 N. This supports the conclusion that, under the higher load, the mechanical load-bearing capacity of the substrate and the ability of the SiC nanofibers to restrict plastic deformation of the Mg matrix became the decisive factors. A similar synergistic mechanism has been described for hybrid Mg-SiC-graphite composites, in which SiC particles acted as load-bearing elements restricting subsurface plastic deformation, while graphite promoted the formation of a stable low-shear tribolayer [9].

Figure 6 shows the surface topography of the materials after tribological testing against a ZrO_2 ceramic ball under a load of 3 N and after 1000 reciprocating strokes/cycles. The axonometric 3D representations of the wear tracks provided spatial information on the width, depth, and morphology of the worn areas. At a load of 3 N, the unreinforced H1 material exhibited a wide and distinctly deepened wear track with an uneven bottom and local material pile-up along the sides. This morphology is consistent with intensive microploughing, plastic flow of the Mg matrix, and delamination of the surface layers. In contrast, H3 exhibited a significantly shallower and more compact wear track, indicating more effective mechanical support of the surface and a more stable carbon-oxide tribofilm. The mildest topographical wear trace was observed for H6, where the wear track was only weakly developed and the volumetric material loss was the lowest. At a load of 5 N, the wear track on H1 became markedly deeper and wider, reflecting intensified plastic deformation and material removal. At 5 N, H3 exhibited a clearly developed wear track with a more pronounced depression than at 3 N, which is consistent with tribofilm destabilization and the sharp increase in wear rate. H6 also showed the mildest topographical wear trace at 5 N. Although the wear track was clearly visible, it remained shallower and less severe than in H1 and H3, confirming the beneficial effect of the higher SiC nanofiber content on the load-bearing capacity of the composite matrix. A similar beneficial effect of hybrid SiC-carbon reinforcement on the wear resistance of the Mg matrix, as well as a transition toward abrasive and delamination mechanisms at increased contact load, was reported by Kavimani et al. [11]. The axonometric maps therefore support the conclusion that, under both loads, the geometrical severity of the wear track decreased in the order H1 > H3 > H6. At 3 N, this trend was mainly reflected in the minimal volumetric material loss of the composites, whereas at 5 N the dominant advantage of H6 was its higher resistance to counterbody penetration and its lower tendency toward large-scale plastic surface damage.

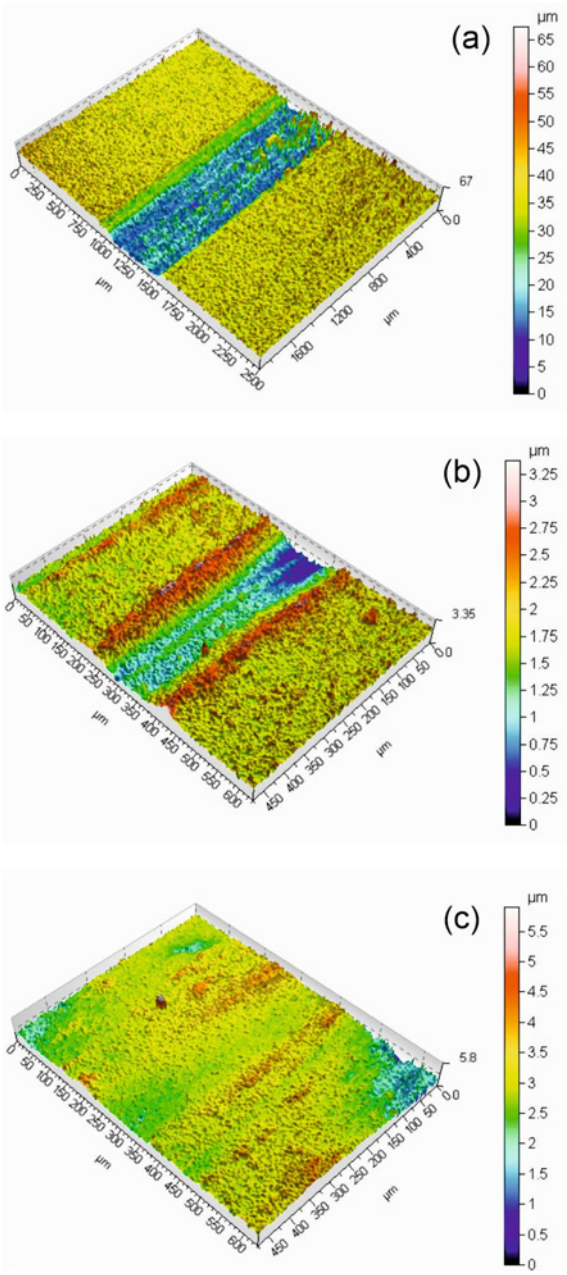


Fig. 6. Axonometric view of the topography of the friction paths of Mg (a), Mg-3 wt.% SiC_{nf}-1 wt.% GNP composite (b), and Mg-6 wt.% SiC_{nf}-1 wt.% GNP composite (c) after translational slip testing against a ZrO_2 ceramic ball.

4. Conclusions

1. SPS processing produced a network microstructure in the H3 and H6 composites, with SiC nanofibers and GNPs preferentially distributed along the interfaces of Mg-rich regions. The addition of 3 wt.% SiC_{nf} and 1 wt.% GNPs increased the average microhardness from 61.8 ± 3.4 HV0.1 for H1 to 65.6 ± 4.7 HV0.1 for H3. Increasing the SiC_{nf} content to 6 wt.% resulted in a thicker and more continuous reinforcement network, accompanied by greater microstructural heterogeneity and local agglomeration, while the microhardness decreased slightly to 62.9 ± 3.9 HV0.1. These results indicate that local microhardness alone does not fully describe the mechanisms governing tribological resistance.

2. The most favorable friction behavior at 3 N was exhibited by the H3 composite. Both H3 and H6 maintained a stable low-friction regime with a coefficient of approximately 0.15–0.17 throughout all 1000 cycles, whereas tribofilm failure occurred in unreinforced H1 after approximately 450 s, followed by an increase in the coefficient of friction above 0.30. The slightly lower friction of H3 compared with H6 indicates a more favorable balance between mechanical support of the tribofilm and the generation of hard abrasive particles.

3. The highest load-bearing capacity at 5 N was demonstrated by the H6 composite. The low-friction regime persisted for approximately 270 s in H1, 680 s in H3, and 920 s in H6. The higher SiC_{nf} content therefore markedly delayed tribofilm failure by restricting counterbody penetration and large-scale plastic deformation of the Mg matrix.

4. The lowest wear rates under both applied loads were obtained for the composite containing 6 wt.% SiC_{nf} and 1 wt.% GNPs. Compared with unreinforced Mg, the wear rate was reduced by approximately > 99 % at 3 N and 94 % at 5 N. The improved wear resistance was associated with the formation of a dynamic carbon-oxide mechanically mixed layer containing graphite, GNPs, Mg oxide products, and fine wear debris, mechanically supported by the SiC nanofibers. However, local pull-out or fragmentation of the SiC reinforcement could simultaneously promote three-body abrasion.

Acknowledgements

This work was supported by the Slovak Scientific Grant Agency (VEGA), project VEGA 2/0157/26.

References

[1] M. Arab, S. P. H. Marashi, Effect of graphene nanoplatelets (GNPs) content on improvement of mechanical and tribological properties of AZ31 Mg matrix nanocomposite, Tribology International 132 (2019) 1–10. https://doi.org/10.1016/j.triboint.2018.11.023

[2] L. Wu, R. Wu, L. Hou, J. Zhang, M. Zhang, Microstructure, mechanical properties and wear performance of AZ31 matrix composites reinforced by graphene nanoplatelets (GNPs), Journal of Alloys and Compounds 750 (2018) 530–536. https://doi.org/10.1016/j.jallcom.2018.04.035

[3] T. Lu, M. Zhou, L. Ren, L. Fan, Y. Guo, X. Qu, H. Zhang, X. Lu, G. Quan, Effect of graphene nanoplatelets content on the mechanical and wear properties of AZ31 alloy, Metals 10 (2020) 1265. https://doi.org/10.3390/met10091265

[4] M. E. Turan, Y. Sun, Y. Akgul, Y. Turen, H. Ahlatci, The effect of GNPs on wear and corrosion behaviors of pure magnesium, Journal of Alloys and Compounds 724 (2017) 14–23. https://doi.org/10.1016/j.jallcom.2017.07.022

[5] M. Shahin, K. Munir, C. Wen, Y. Li, Nano-tribological behavior of graphene nanoplatelet-reinforced magnesium matrix nanocomposites, Journal of Magnesium and Alloys 9 (2021) 895–909. https://doi.org/10.1016/j.jma.2020.10.001

[6] S. Kandemir, S. Yöyler, R. Kumar, M. Antonov, H. Dieringa, Effect of graphene nanoplatelet content on mechanical and elevated-temperature tribological performance of self-lubricating ZE10 magnesium alloy nanocomposites, Lubricants 12 (2024) 52. https://doi.org/10.3390/lubricants12020052

[7] A. Das, S. P. Harimkar, Effect of graphene nanoplate and silicon carbide nanoparticle reinforcement on mechanical and tribological properties of spark plasma sintered magnesium matrix composites, Journal of Materials Science & Technology 30 (2014) 1059–1070. https://doi.org/10.1016/j.jmst.2014.08.002

[8] K. Soorya Prakash, P. Balasundar, S. Nagaraja, P. M. Gopal, V. Kavimani, Mechanical and wear behaviour of Mg-SiC-Gr hybrid composites, Journal of Magnesium and Alloys 4 (2016) 197–206. https://doi.org/10.1016/j.jma.2016.08.001

[9] A. E. A. Al-Maamari, A. K. M. A. Iqbal, D. M. Nuruzzaman, Mechanical and tribological characterization of self-lubricating Mg-SiC-Gr hybrid metal matrix composite fabricated via mechanical alloying, Journal of Science: Advanced Materials and Devices 5 (2020) 535–544. https://doi.org/10.1016/j.jsamd.2020.09.002

[10] V. Kavimani, K. S. Prakash, T. Thankachan, Experimental investigations on wear and friction behaviour of SiC@r-GO reinforced Mg matrix composites produced through solvent-based powder metallurgy, Composites Part B: Engineering 162 (2019) 508–521. https://doi.org/10.1016/j.compositesb.2019.01.009

[11] V. Kavimani, K. S. Prakash, M. S. Starvin, B. Kalidas, V. Viswamithran, S. R. Arun, Tribo-surface characteristics and wear behaviour of SiC@r-GO/Mg composite worn under varying control factor, Silicon 12 (2020) 29–39. https://doi.org/10.1007/s12633-019-0095-2

[12] V. Kavimani, K. S. Prakash, T. Thankachan, Surface characterization and specific wear rate prediction of r-GO/AZ31 composite under dry sliding wear

condition, Surfaces and Interfaces 6 (2017) 143–153. https://doi.org/10.1016/j.surfin.2017.01.004

[13] M. Srinivasan, C. Loganathan, M. Kamaraj, Q. B. Nguyen, M. Gupta, R. Narayanasamy, Sliding wear behaviour of AZ31B magnesium alloy and nanocomposite, Transactions of Nonferrous Metals Society of China 22 (2012) 60–65. https://doi.org/10.1016/S1003-6326(11)61140-0

[14] A. Matin, F. F. Saniee, H. R. Abedi, Microstructure and mechanical properties of Mg/SiC and AZ80/SiC nanocomposites fabricated through stir casting method, Materials Science and Engineering A 625 (2015) 81–88. https://doi.org/10.1016/j.msea.2014.11.050

[15] D. Penther, A. Ghasemi, R. Riedel, C. Fleck, S. Kamrani, Effect of SiC nanoparticles on manufacturing process, microstructure and hardness of Mg–SiC nanocomposites produced by mechanical milling and hot extrusion, Materials Science and Engineering A 738 (2018) 264–272. https://doi.org/10.1016/j.msea.2018.09.106

[16] S. Banerjee, P. Sahoo, J. P. Davim, Tribological characterisation of magnesium matrix nanocomposites: A review, Advances in Mechanical Engineering 13 (2021) 1–39. https://doi.org/10.1177/16878140211009025

[17] H. Ahmadian, T. Zhou, A. Alansari, A. Senthil Kumar, A. Fathy, M. Elmahdy, Q. Yu, W. Guo, Microstructure, mechanical properties and wear behavior of Mg matrix composites reinforced with Ti and nano SiC particles, Journal of Materials Research and Technology 31 (2024) 4088–4103. https://doi.org/10.1016/j.jmrt.2024.07.125

[18] K. S. Sridhar Raja, V. Kishorekumar, E. Mathan, K. Subbiah, H. Janarthanam, S. Kumar Jayapalan, M. Sangeetha, Wear optimization of graphene reinforced magnesium AZ31 composite using Taguchi design, AIP Conference Proceedings 2311 (2020) 080005. https://doi.org/10.1063/5.0034025

[19] M. Abdulgadir, B. Demir, M. Turan, Hybrid reinforced magnesium matrix composites (Mg/SiC/GNPs): Drilling investigation, Metals 8 (2018) 215. https://doi.org/10.3390/met8040215

[20] S. Ayyanar, R. Kaliyamoorthy, A. Gnanavelbabu, P. Loganathan, Friction and wear properties of AZ91D magnesium composites under varying load and tungsten disulphide solid lubricant, Industrial Lubrication and Tribology 77 (2025) 1380–1392. https://doi.org/10.1108/ILT-10-2024-0373